euspen's 24th International Conference & Exhibition, Dublin, IE, June 2024
www.euspen.eu

# High speed air bearing spindle for ultra precision machining

Byron Knapp, Dan Oss, and Dave Arneson

*Professional Instruments Company, Hopkins, Minnesota, USA*

bknapp@airbearings.com

**Abstract**

Increasing demands for deterministic direct machining of infrared optics and molds require a precision air bearing spindle with high stiffness capable of higher cutting speeds. This paper describes design and testing of a new porous graphite air bearing spindle for diamond machining capable of 18 000 RPM. The design uses porous graphite journal sleeves and compound compensated captured thrusts. The spindle is water-cooled to maintain thermal stability and vacuum is supplied to the chuck for workpiece fixturing via a non-contact rotary union. Proper testing techniques and apparatus required for critical aspects of an ultra-precision spindle are described. Static stiffness testing demonstrates radial stiffness at the nose better than 50 N/µm and axial stiffness of 280 N/µm. Dynamic response shows the first natural frequency is highly damped and above 1 400 Hz. Spindle error motions less than 5 nm are demonstrated enabling optics with sub-micrometer form and sub-nanometer finish.

Keywords: porous graphite air bearing spindle, infrared optics, micro optics

## 1. Background

The ultra-precision air bearing work spindle shown in Figure 1 has been newly developed to address the increasing number of applications requiring infrared and micro optics [1]. Brittle single crystal semiconductors and micro optic molds and can be machined at higher spindle speeds to reduce brittle fracture [2] and improve productivity [3]. However, rotational speed is often limited to 10 000 RPM in an effort to mitigate dynamic spindle errors [4, 5]. To address this need, a new porous graphite air bearing spindle has been developed capable of 18 000 RPM with high stiffness and nanometer-level errors beyond the current state-of-the-art.

With higher speeds, reduction and control of heat generated due to shearing is a primary design consideration. Petrov's equations for the journal and thrust bearings are [6]:

$$P_J = \frac{\pi^3}{450}\frac{\mu\ell}{h}r^3N^2$$

where $P_J$ is the power to shear the journal air film, $\mu$ is the absolute viscosity, $r$ is the shaft radius, $h$ is the film thickness, $\ell$ is the journal length, and $N$ is the rotational speed in units of revolutions per minute.

$$P_T = \frac{\pi^3\mu N^2}{1800h}({r_o}^4 - {r_i}^4)$$

where $P_T$ is the power to shear the thrust air film, $r_i$ is the inner radius of the thrust, and $r_o$ is the outer radius of the thrust. With 8 µm air films to provide high stiffness, 200 W due to shearing is expected at 18 000 RPM which can be managed using water cooling. The spindle housing (aluminium) has a larger coefficient of thermal expansion than the shaft (stainless steel) to prevent thermal runaway. Due to the difference in thermal coefficients, as the spindle warms up from shearing, the air film thickness increases resulting in less heat and a stable thermal system.

The cross section in Figure 2 shows porous graphite journals and compound compensated captured thrusts (grooved thrust face fed by journal flow). A brushless permanent magnet motor and a 1 650 line-count encoder are mounted directly to the spindle shaft. Vacuum is supplied to the chuck for workholding via a non-contact rotary union.

**Figure 1.** Porous graphite air bearing spindle for diamond turning.

## 2. Static stiffness

Static stiffness is a crucial indicator for spindles to be used in precision machining applications—particularly central stiffness under light cutting loads. Specially-built hardware to measure radial load capacity and radial static stiffness is shown in Figure 3. An air bearing piston pulls the rotor at the nose of the spindle in the radial direction. In a separate metrology loop, a twisted band Abramson movement indicator (CEJ Mikrokator) with 250 nm resolution measures radial displacement of the rotor. Ultimate radial load capacity at the spindle nose is 700 N with 0.7 MPa inlet pressure. Resulting radial stiffness at the nose is 54 N/µm with 0.7 MPa inlet pressure. The stiffness is linear through the load range which is critical especially in the low-load region typical of precision machining.

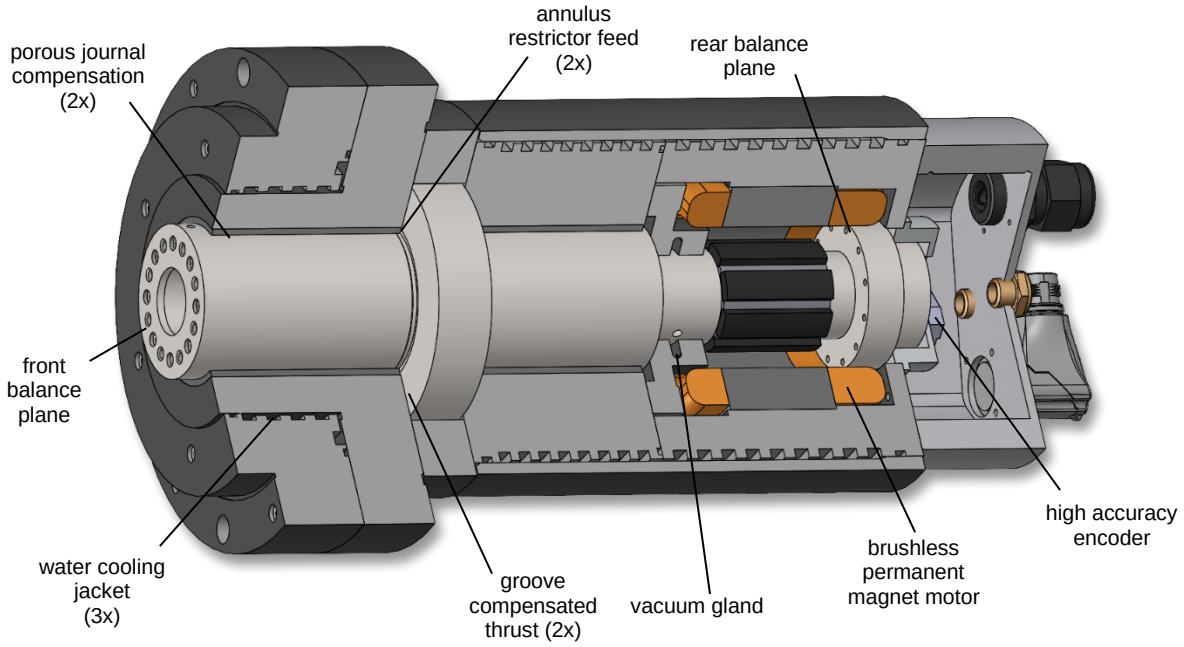


**Figure 2.** Cross section of porous graphite work spindle for diamond machining.

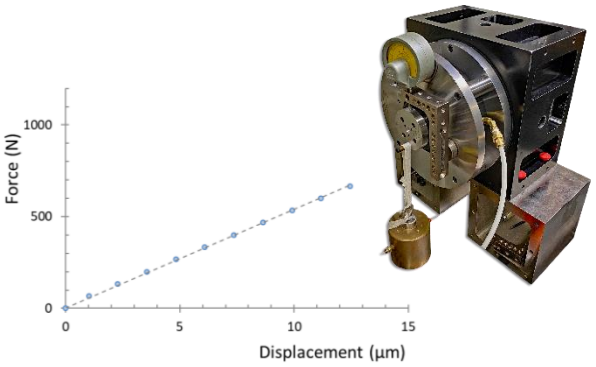


**Figure 3.** Radial stiffness and load capacity at the spindle nose is 54 N/µm and 700 N with 0.7 MPa inlet pressure.

Hardware to measure axial load capacity and axial static stiffness is shown in Figure 4. In this test, an air bearing piston pushes the rotor at the top of the spindle in the axial direction. At the bottom of the setup, in a separate metrology loop, axial displacement of the rotor is recorded. Ultimate axial load capacity is 1 450 N and axial stiffness is 280 N/µm with 0.7 MPa inlet pressure.

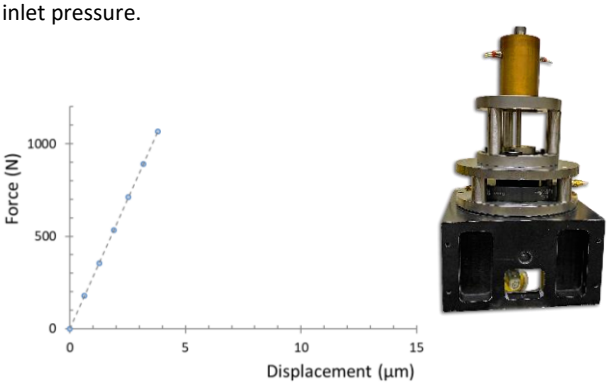


**Figure 4.** Axial stiffness and load capacity is 280 N/µm and 1 450 N with 0.7 MPa inlet pressure.

## 3. Dynamic stiffness

Modal analysis is used to determine dynamic response with natural frequencies and mode shapes in the radial and axial directions. The spindle is supported on compliant foam to minimize boundary condition influences. An impact hammer (Kistler 500 N) excites the housing in the radial direction whilst an accelerometer (Kister K-Shear 25g), attached to the rotor, measures the radial direction response. A 24-bit dynamic signal analyzer (Data Physics SignalCalc Ace) records excitation and response to calculate frequency response functions. The radial response is dominated by a heavily damped mode at 1 400 Hz.

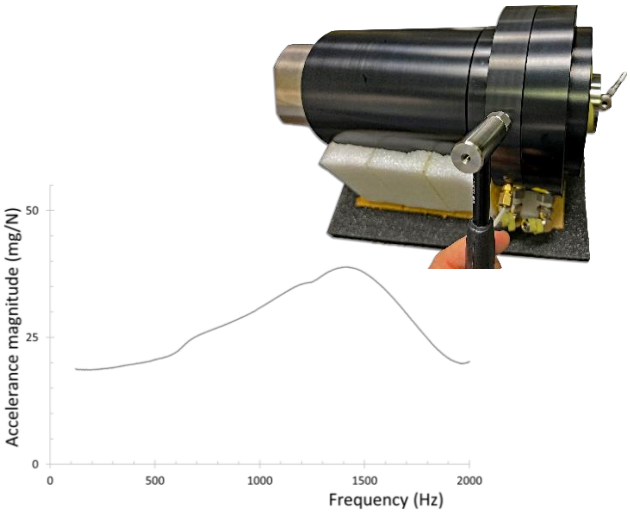


**Figure 5.** Radial direction frequency response function shows a highly damped mode at 1 400 Hz.

A modal impact test in the axial direction and resulting frequency response is shown in Figure 6. For this test, an impact hammer excites the rotor in the axial direction while an accelerometer mounted to the structure measures the axial response. With an inlet pressure of 0.7 MPa, the first mode is highly damped and again at 1 400 Hz. Heavily damped modes in the axial direction help prevent axial spoking (star pattern) in an optical surface machined with this spindle [7].

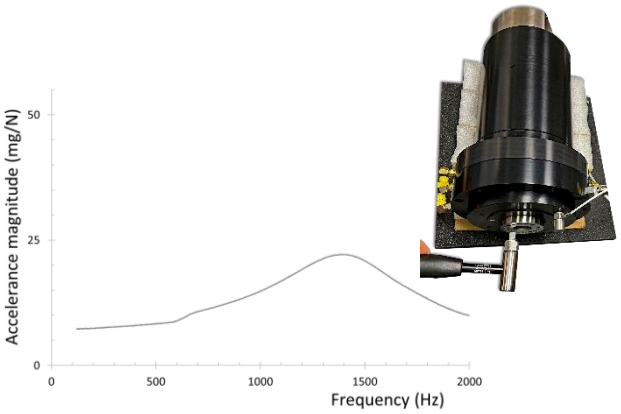


**Figure 6.** Axial direction frequency response function shows a highly damped mode at 1 400 Hz.

## 4. Error motion

Precision spindle metrology is typically accomplished by measuring the surface of an artifact mounted to a spindle [8]. This is complicated by the fact that artifact out-of-roundness often exceeds error of a precision spindle and separation techniques must be used to extract the desired measurement. Donaldson's reversal technique provides an elegant mathematical solution for separating spindle radial error motion from artifact form error [9]. However, in practice, measurement accuracy of this reversal technique suffers due to a variety of potential error sources. To address this issue, Whitehouse developed a multiprobe technique which avoids some of the problems with reversal [10].

Bespoke tooling to implement a modified version of Whitehouse's multiprobe radial error separation is shown in Figure 7. Harmonic suppression is minimized by using angular indexing of a single capacitive sensor at asymmetrically spaced angles of 0°, 99.844° and 202.5° [11]. Axial error motion is also measured with this tooling at a single angular orientation because separation is not required for axial measurements.

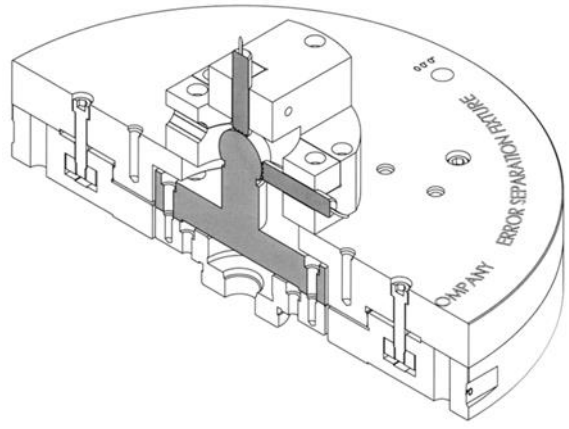


**Figure 7.** Bespoke multiprobe error separation tooling with 25 mm diameter spherical artifact.

In Figure 8, a capacitive sensor (Lion Precision C23-C, 0.4 µm/V) targets a 25 mm diameter lapped sphere. The sensor amplifier (Lion Precision CPL190) incorporates a 15 kHz first-order, low-pass analog filter with linear phase response. The data acquisition system (Lion Precision SEA) is triggered by the 1 650 line-count encoder, providing immunity to synchronization errors caused by speed variation. A low-pass digital filter with a 150 UPR cut-off is applied to the axial and radial error motion plots. Total radial and axial error motions less than 5 nm are shown in Figure 9 and Figure 10.

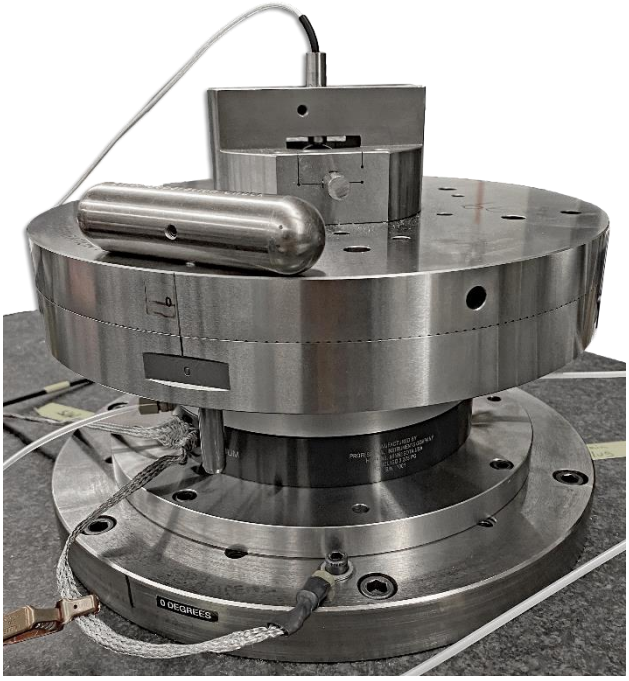


**Figure 8.** Setup for radial and axial spindle error measurement.

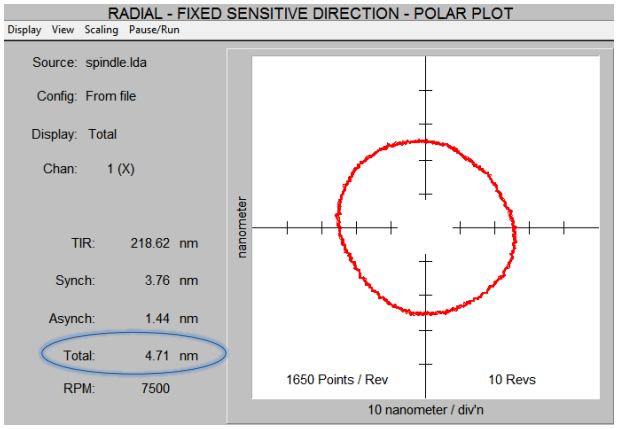


**Figure 9.** Radial spindle error motion after separation.

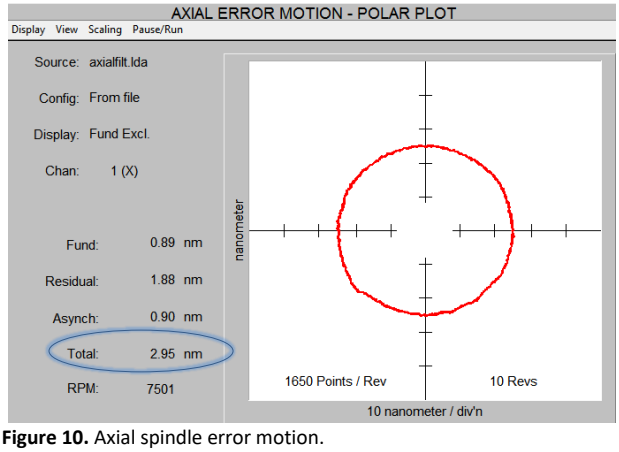


**Figure 10.** Axial spindle error motion.

## 5. Summary

Proper testing techniques of three critical aspects of a new porous graphite air bearing spindle for diamond machining are revealed. Static stiffness and load capacity is demonstrated by using air pistons to apply a load while recording displacement in a separate metrology loop. With modal analysis, dynamic response is shown to have a high first natural frequency that is well-damped. Finally, bespoke tooling is used to perform multiprobe error separation with results better than 5 nm.

## 6. Conclusion

An increasing number of small optics must be machined at higher spindle speeds for increased productivity. A new porous graphite air bearing workholding spindle which extends the current state-of-the-art has been developed to address this need. Static stiffness testing demonstrates radial stiffness at the nose and axial stiffness better than 50 N/µm and 280 N/µm respectively. The dynamic response shows the first natural frequency is highly damped and above 1 400 Hz. Equipment and techniques to measure radial and axial spindle error motion less than 5 nm are demonstrated.

## References


[1] MA Davies et al. Application of precision diamond machining to the manufacture of microphotonics components. *Proc. SPIE 5183*, 2003.

[2] M Tunesi et al. Effect of cutting speed in single point diamond turning of (100)Ge. *Manufacturing Letters*. **38**: 15-18, 2023.

[3] E Brinksmeier and L Schönemann (Eds.) Ultra-precision High Performance Cutting. Report of DFG Research Unit FOR 1845. Springer Nature Switzerland AG Cham: 2020.

[4] P Huang et al. Investigation of the effects of spindle unbalance induced error motion on machining accuracy in ultra-precision diamond turning. *Int J of Machine Tools & Manufacture*. **94**: 48–56, 2015.

[5] D Huo and K Cheng. Micro-Cutting: Fundamentals and Applications - Diamond turning and micro turning, 153-183, 2013.

[6] NP Petrov. Friction in Machines and The Effect of The Lubricant *Inzhenernii Zhurnal*, Volume **1-4**, 1883.

[7] M Tauhiduzzaman et al. Form error in diamond turning. *Precision Engineering*, **42**: 22-36, 2015.

[8] E Marsh. Precision Spindle Metrology, Second Edition. Destech Publications, Inc. Lancaster, PA: 2010.

[9] R Donaldson. A simple method for separating spindle error from test ball roundness error. *Annals of CIRP*, **21**(1):125-126, 1972.

[10] D Whitehouse. Some Theoretical Aspects of Error Separation Techniques in Surface Metrology. *J. of Phys. E: Sci. Inst.* **9**:531-536, 1976.

[11] E Marsh et al. A Comparison of Reversal and Multiprobe Error Separation. *Precision Engineering*. **34**:85-91, 2010.